

Title:

Dynamical stability and quantum chaos of ions in a linear trap

Author(s):

G. P. Berman, D. F. V. James, R. J. Hughes,
M. S. Gulley, M. H. Holzscheiter, and G. V. López

Submitted to:

<http://lib-www.lanl.gov/cgi-bin/getfile?00796984.pdf>

Dynamical stability and quantum chaos of ions in a linear trap

G. P. Berman,^{1,*} D. F. V. James,² R. J. Hughes,³ M. S. Gulley,⁴ M. H. Holzscheiter,³ and G. V. López⁵

¹Group T-13 and CNLS, University of California, Los Alamos National Laboratory, Los Alamos, New Mexico 87545

²Group T-4, University of California, Los Alamos National Laboratory, Los Alamos, New Mexico 87545

³Group P-23, University of California, Los Alamos National Laboratory, Los Alamos, New Mexico 87545

⁴Group P-25, University of California, Los Alamos National Laboratory, Los Alamos, New Mexico 87545

⁵Departamento de Física, Universidad de Guadalajara, Corregidora 500, S.R. 44420, Guadalajara, Jalisco, Mexico

(Received 19 March 1999; published 7 January 2000)

The realization of a paradigm chaotic system, namely, the harmonically driven oscillator, in the quantum domain using cold trapped ions driven by lasers is theoretically investigated. The simplest characteristics of regular and chaotic dynamics are calculated. The possibilities of experimental realization are discussed.

PACS number(s): 42.50.Vk, 05.45.Mt, 32.80.Pj

I. INTRODUCTION

One of the major difficulties in developing quantum technologies, such as quantum computers [1,2], is the different kinds of specifically quantum dynamical instabilities that can occur due to interactions between different degrees of freedom and resonant interaction with the external fields. These instabilities differ from dynamical instabilities in classical systems, which are usually connected with the strong dependence of trajectories on the initial conditions and on the values of parameters. Small variations of initial conditions or parameters lead to large deviations in the time of the corresponding trajectories. If the speed of this deviation is exponential, the system becomes chaotic, and the appropriate methods of description are statistical rather than deterministic. However, for quantum systems, the notion of a trajectory is not well defined. This is one of the main reasons why most of the well-developed methods for stability analysis cannot be directly applied to quantum systems. Moreover, as was first shown theoretically by Berman and Zaslavsky [3,4] (see also Ref. [5]), even in a “deep” quasiclassical region, classically chaotic systems can have a quantum dynamics that is very different from the corresponding classical dynamics.

Another important phenomenon which takes place in quantum systems which are classically chaotic is *quantum nonlinear resonance* (QNR), which was first introduced and investigated theoretically by Berman and Zaslavsky [6]. QNR’s are quantum manifestation of nonlinear resonances which play very important role in classically chaotic systems [7–10]. Interactions of QNR’s are known to be intimately connected to the transition to quantum chaos [11–17]. In the simplest situations, QNR’s occur when a bound quantum system whose energy levels are not equally spaced is driven by a resonant perturbation. A QNR is characterized by two main parameters: the number of quasienergy levels, δn , which are “trapped” in the potential well of the resonance, and the characteristic frequency of slow phase oscillations, Ω_{ph} . Isolated QNR’s imply stable quantum dynamics; overlapping QNR’s cause a transition to quantum chaos. QNR’s

are very general phenomena in nonintegrable quantum systems, and can be thought of as “quasiparticles” of quantum chaos (for more details, see Chap. 9 of Reichl’s recent book [18], which is devoted to the transition to quantum chaos caused by interaction of QNR’s). Until now, QNR effects have been experimentally investigated using Rydberg atoms in a resonant microwave field [19]. Understanding the instabilities connected with overlapping QNR’s is important for fundamental problems related to the transition to quantum chaos, and for the design of experimental devices (such as quantum computers based on ion traps) in which these instabilities may cause significant problems. To study the characteristic parameters of both isolated QNR’s and the problems related to interaction of QNR’s, it is important to choose a model which (a) involves a regulated (and relatively small) number of interacting QNR’s; and (b) can be implemented experimentally in quantum and quasiclassical regions of parameters.

In this paper we introduce a quantum model which is convenient for the investigation of quantum dynamical instabilities and the transition to quantum chaos based on the overlapping of QNR’s. The model consists of a single ion confined in a radio-frequency Paul trap, which interacts with a resonant laser field. In the classical limit, this model reduces to the well-known model of a linear oscillator interacting with a plane electromagnetic wave, and was investigated in Ref. [20–22] (see also references therein). The main advantage of our model is that the number of interacting QNR’s can be regulated, for example, by varying the intensity of the laser radiation, which is difficult to achieve in other models based on the kicked interaction [23–28].

Devices based on trapped ions have been used to investigate experimentally fundamental aspects of quantum mechanics [29,30], as well as for important technological applications such as optical frequency standards [31] and quantum computing [1,32]. Ions are confined by a combination of a rotating quadrupole potential (induced by the rod electrodes) and a weak electrostatic potential (induced by the conical endcap electrodes). The ions, once trapped, can be cooled by standard Doppler cooling and by an optical pumping method (“sideband cooling”), which can cool multiple ions down to the quantum-mechanical ground state of the trapping potential. In an ion trap quantum computer, infor-

*Author to whom correspondence should be addressed. Electronic address: Electronic address: gpb@lanl.gov

mation can be stored in the internal quantum states of the ions (which constitute the quantum bits, or “qubits” of the computer), and, using ultranarrow bandwidth lasers, quantum gate operations can be realized between pairs of qubits using quantum states of the collective motion of the ions in the harmonic confining potential as a quantum information bus [33]. As such devices are specifically designed to investigate experimentally the preparation, evolution, and measurement of quantum systems with large dimension Hilbert spaces, the linear ion trap is an ideal apparatus to investigate the problems of quantum-dynamical stability, the transition to quantum chaos, and the spectroscopy of quantum nonlinear resonances. In this paper, we present the main elements of the derivation of our model—a quantum linear oscillator driven by a monochromatic wave, and the preliminary analytical and numerical results on the classical and quantum dynamics in different regions of parameters.

The paper is organized as follows. In Sec. II, the theory of how a trapped ion can be driven by laser fields in the manner of the harmonically driven oscillator is described in detail. We decided to present a detailed derivation of the Hamiltonian because it is important for a justification of the model we use and for fitting the parameters in the experiments which are planned in the future. It should be noted in particular how similar the arrangement and laser requirements are to those employed in ion trap quantum computer experiments. In Sec. III, the *classical* theory of the harmonically driven oscillator is discussed; the quantum theory is described in Sec. IV. The connection of this system with the solid-state Anderson localization model is described in Sec. V. The results of numerical simulations are presented in Sec. VI. We conclude this paper with a brief discussion of the possibilities for experimental verifications.

II. RAMAN INTERACTIONS OF LASERS AND TRAPPED IONS

In this section we derive the Hamiltonian describing a trapped ion interacting with laser fields in the manner of a harmonically driven oscillator. One of the goals of the present investigation is a theoretical analysis of an experimentally realizable dynamic system, and, in order to facilitate the interface between theory and experiment, we describe the laser-ion interaction in some detail. A single ion confined in a linear rf trap may be described by an effective Hamiltonian given by the formula

$$\hat{H} = \frac{1}{2m}\hat{p}^2 + \frac{1}{2}m\omega^2\hat{x}^2 + \hat{H}_I, \quad (2.1)$$

where m is the mass of the ion, \hat{x} (\hat{p}) is the position (momentum) operator for the ion, and ω is the angular trapping frequency. We are only considering motion of the ion along one direction, namely, the axis of weak confinement of the trap; the ion is strongly confined along the other two directions, transverse to the axis, and so we will assume that the motion in those directions can be neglected (see Fig. 1).

We will employ the interference of two laser beams acting on the ion to realize experimentally our desired interac-

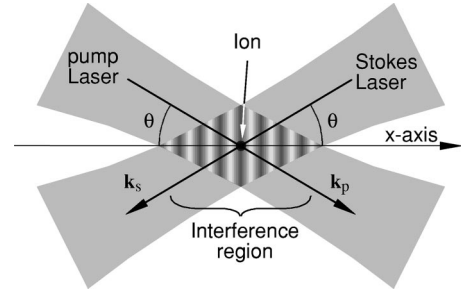


FIG. 1. A schematic diagram of an ion in a linear trap to illustrate the notation and configurations of the laser fields.

tion Hamiltonian \hat{H}_I . Such Raman interactions between lasers and ions are a standard technique, and are described in detail elsewhere [34]. The ion, confined in the harmonic trapping potential, will have many quantum levels associated with both internal (atomic) variables and external (motional) degrees of freedom. We will confine our attention to two manifolds of such states, separated in energy by an appreciable amount (see Fig. 2). What we have in mind is a lower manifold consisting of the magnetic sublevels of our ion, each level having a series of sidebands associated with excitation of quanta of the external harmonic oscillations; the upper manifold would then be the sublevels of an excited state of the ion, with similar sidebands. The lasers with which the ion is interacting will be detuned from the optical transition between the upper and lower levels, so that there is a negligible probability of any of these levels becoming excited: the lasers only cause a redistribution of population among the lower manifold of levels. The upper levels may then be adiabatically eliminated from the problem, and one can therefore show that the matrix elements of the effective interaction Hamiltonian for the lower manifold is given by the formula [34]

$$\langle M | \hat{H}_I | N \rangle = - \sum_L \sum_{\alpha, \alpha'} \frac{\Omega_{ML}^{(\alpha)} \Omega_{NL}^{(\alpha')*}}{4\hbar(\omega_L - \omega_N - \omega_{\alpha'})} \times \exp[i(\omega_{\alpha} - \omega_{\alpha'})t], \quad (2.2)$$

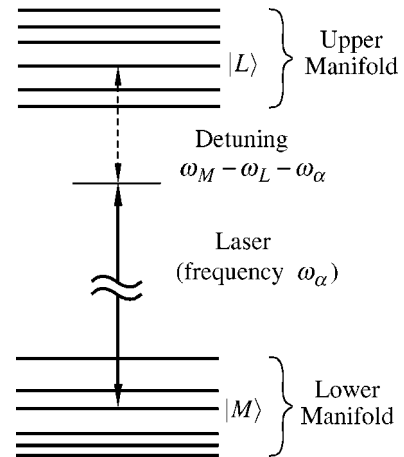


FIG. 2. A schematic illustration of the energy levels of a trapped ion.

where the sum involving u is over all of the upper manifold levels and the two sums involving α and α' are over all of the applied laser fields, the Rabi frequency of the α th laser being defined by

$$\hbar\Omega_{ML}^{(\alpha)} = \langle M | \hat{d}_i E_i^{(\alpha)}(\hat{\mathbf{r}}) | L \rangle. \quad (2.3)$$

In Eq. (2.3), \hat{d}_i is the i th component of the dipole moment operator [$i=(1,2,3)$, standing for the three Cartesian components of a vector, and summation over repeated indices being implied], $E_i^{(\alpha)}$ is the i th component of the electric field from the α th laser (which is a function of the ion's position operator, $\hat{\mathbf{r}}$), $\hbar\omega_M$ is the energy of the M th lower manifold level, $\hbar\omega_L$ is the energy of the L th upper manifold level, and ω_α is the angular frequency of the α th laser.

To proceed, we will make a distinction between internal and external degrees of freedom. We can form a basis set for the Hilbert space from a tensor product of a set of internal quantum levels with a basis set for the external degrees of freedom (for example, the Fock states of the harmonic oscillator). The set of internal states will be divided between the upper and lower manifolds. Thus we will make the substitution

$$|L\rangle \rightarrow |\lambda\rangle |l\rangle, \quad (2.4)$$

$$|M\rangle \rightarrow |\mu\rangle |m\rangle, \quad (2.5)$$

$$|N\rangle \rightarrow |\nu\rangle |n\rangle, \quad (2.6)$$

where $|m\rangle$, $|n\rangle$, and $|l\rangle$ are members of the basis states for the motion degrees of freedom, $|\lambda\rangle$ is a member of the upper internal manifold, and $|\mu\rangle$ and $|\nu\rangle$ are members of the lower internal manifold. In this notation, the matrix elements of the Hamiltonian equation (2.2) become:

$$\begin{aligned} & \langle \mu | \langle m | \hat{H}_I | n \rangle | \nu \rangle \\ &= - \sum_{\lambda} \sum_l \sum_{\alpha, \alpha'} \frac{\langle \mu | \hat{d}_i | \lambda \rangle \langle \lambda | \hat{d}_j | \nu \rangle}{4\hbar(\omega_\lambda - \omega_\nu - \omega_{\alpha'} + \omega_l - \omega_n)} \\ & \quad \times \langle m | E_i^{(\alpha)}(\hat{\mathbf{r}}) | l \rangle \langle l | E_j^{(\alpha')}(\hat{\mathbf{r}}) | n \rangle \exp[i(\omega_\alpha - \omega_{\alpha'})t]. \end{aligned} \quad (2.7)$$

The average detuning of the λ th upper manifold level is defined to be

$$\Delta_\lambda = \omega_\lambda - \bar{\omega}_\nu - \bar{\omega}_\alpha, \quad (2.8)$$

where $\hbar\bar{\omega}_\nu$ is the average energy of the lower manifold and $\bar{\omega}_\alpha$ is the average of the laser frequencies. We will assume that, in the denominator of the fraction appearing in Eq. (2.7), we can make the following approximation:

$$\omega_\lambda - \omega_\nu - \omega_{\alpha'} + \omega_l - \omega_n \approx \Delta_\lambda. \quad (2.9)$$

If we use the completeness property of the external basis states (i.e., $\sum_l |l\rangle \langle l| = \hat{I}$, where \hat{I} is the identity operator), then

we obtain the following formula for the Hamiltonian operator for the lower manifold states:

$$\hat{H}_I = \sum_{\mu, \nu} \kappa_{\mu, \nu}(\hat{\mathbf{r}}, t) |\mu\rangle \langle \nu|, \quad (2.10)$$

where

$$\kappa_{\mu, \nu}(\hat{\mathbf{r}}, t) = - \sum_{\lambda} \frac{\langle \mu | \hat{d}_i | \lambda \rangle \langle \lambda | \hat{d}_j | \nu \rangle}{4\hbar\Delta_\lambda} E_i(\hat{\mathbf{r}}, t) E_j^*(\hat{\mathbf{r}}, t), \quad (2.11)$$

and the total laser field E_i is the sum of the different laser components:

$$E_i(\hat{\mathbf{r}}, t) = \sum_{\alpha} E_i^{(\alpha)}(\hat{\mathbf{r}}) \exp(i\omega_\alpha t). \quad (2.12)$$

A. Two-level systems

Let us now assume that there are only two internal levels in the lower manifold, which we will denote $|1\rangle$ and $|2\rangle$. As will be discussed below, this is a reasonable assumption to make for the atomic systems we have in mind. Also, we introduce a special coordinate system: the two internal levels are split by a magnetic field acting along the Z axis, which is the axis of quantization for the internal levels of our ion. The other two axes are the X and Y axes. These axes do *not* necessarily coincide with the x , y , and z directions introduced to describe the motion of the ion in the trap. In this case it is convenient to use the Pauli operators for the system:

$$\hat{\sigma}_1 = |1\rangle \langle 2| + |2\rangle \langle 1|, \quad (2.13)$$

$$\hat{\sigma}_2 = i(|1\rangle \langle 2| - |2\rangle \langle 1|), \quad (2.14)$$

$$\hat{\sigma}_3 = |2\rangle \langle 2| - |1\rangle \langle 1|. \quad (2.15)$$

Using these operators the Hamiltonian can be written as

$$\hat{H}_I = h_0(\hat{\mathbf{r}}, t) \hat{I} + h_i(\hat{\mathbf{r}}, t) \hat{\sigma}_i, \quad (2.16)$$

where \hat{I} is the identity operator ($|1\rangle \langle 1| + |2\rangle \langle 2|$), and

$$h_0(\hat{\mathbf{r}}, t) = \frac{1}{2} [\kappa_{1,1}(\hat{\mathbf{r}}, t) + \kappa_{2,2}(\hat{\mathbf{r}}, t)], \quad (2.17)$$

$$h_1(\hat{\mathbf{r}}, t) = \frac{1}{2} [\kappa_{1,2}(\hat{\mathbf{r}}, t) + \kappa_{2,1}(\hat{\mathbf{r}}, t)], \quad (2.18)$$

$$h_2(\hat{\mathbf{r}}, t) = \frac{1}{2i} [\kappa_{1,2}(\hat{\mathbf{r}}, t) - \kappa_{2,1}(\hat{\mathbf{r}}, t)], \quad (2.19)$$

$$h_3(\hat{\mathbf{r}}, t) = \frac{1}{2} [\kappa_{2,2}(\hat{\mathbf{r}}, t) - \kappa_{1,1}(\hat{\mathbf{r}}, t)]. \quad (2.20)$$

For the special case that the lower manifold of internal states consists of two magnetic sublevels of the $^2S_{1/2}$ ground state

of an alkali like ion, and the upper manifold is the two sub-levels of the $^2P_{1/2}$ excited state whose Zeeman splitting is not too large, the atomic matrix elements appearing in Eq. (2.11) can be calculated in closed form. As a result the components of h appearing in Eq. (2.16) reduce to the simple forms (see Appendix A)

$$\begin{aligned} h_0(\hat{\mathbf{r}}, t) &= -\chi |\mathbf{E}(\hat{\mathbf{r}}, t)|^2, \\ h_1(\hat{\mathbf{r}}, t) &= 2\chi \text{Im}\{E_Z(\hat{\mathbf{r}}, t)E_Y^*(\hat{\mathbf{r}}, t)\}, \\ h_2(\hat{\mathbf{r}}, t) &= 2\chi \text{Im}\{E_X(\hat{\mathbf{r}}, t)E_Z^*(\hat{\mathbf{r}}, t)\}, \\ h_3(\hat{\mathbf{r}}, t) &= 2\chi \text{Im}\{E_X(\hat{\mathbf{r}}, t)E_Y^*(\hat{\mathbf{r}}, t)\}, \end{aligned} \quad (2.21)$$

where $\text{Im}\{\dots\}$ is the imaginary part of the quantity in curly brackets, and $\chi = A\pi\epsilon_0/4k_0^3\Delta$ (k_0 and A are, respectively, the wave number and Einstein A coefficient for the transition between the upper and lower manifolds. Δ is the laser detuning and ϵ_0 the permittivity of free space).

The quantity proportional to $h_0(\hat{\mathbf{r}}, t)$ in Eq. (2.16) represents a dynamical effect of the laser fields on the ion which does not cause any effect on its internal degrees of freedom; the term proportional to $h_3(\hat{\mathbf{r}}, t)$ represents an ac Stark shift of the two internal levels; the terms proportional to $h_1(\hat{\mathbf{r}}, t)$ and $h_2(\hat{\mathbf{r}}, t)$ represent transitions between the two levels of the lower manifold. If we make the requirement that the lasers are plane polarized along the axis of quantization Z , then it is clear from the above formulas that $h_1 = h_2 = h_3 = 0$, and only the first term involving h_0 has any effect.

Let us assume that two laser beams, designated the pump (p) and Stokes (s) beams, are present, both plane polarized in the Z direction, i.e.,

$$\begin{aligned} E_X(\hat{\mathbf{r}}, t) &= 0, \\ E_Y(\hat{\mathbf{r}}, t) &= 0, \\ E_Z(\hat{\mathbf{r}}, t) &= E^{(p)} \exp[-i(\mathbf{k}_p \cdot \hat{\mathbf{r}} - \omega_p t)] + E^{(s)} \\ &\quad \times \exp[-i(\mathbf{k}_s \cdot \hat{\mathbf{r}} - \omega_s t)]. \end{aligned} \quad (2.22)$$

The interaction Hamiltonian in this case is given by

$$\begin{aligned} \hat{H}_I &= \chi \{|E^{(p)}|^2 + |E^{(s)}|^2 + 2|E^{(p)}E^{(s)*}| \\ &\quad \times \cos[(\mathbf{k}_p - \mathbf{k}_s) \cdot \hat{\mathbf{r}} - (\omega_p - \omega_s)t + \phi]\}, \end{aligned} \quad (2.23)$$

where $\phi = \text{Arg}\{E^{(p)}E^{(s)*}\}$ is the phase difference between the two lasers. The constant terms involving $|E^{(p)}|^2$ and $|E^{(s)}|^2$ have no effect on the evolution, and so will be neglected. Thus the full Hamiltonian, including the effect of the harmonic evolution of the ion along the weak axis of the trap (but excluding the internal free evolution), is

$$\hat{H} = \frac{\hat{p}^2}{2m} + \frac{m\omega^2\hat{x}^2}{2} + \frac{\varepsilon}{k} \cos(k\hat{x} - \Omega t), \quad (2.24)$$

where $\Omega = \omega_p - \omega_s$. The parameters ε and k , which will feature prominently in what follows, are given by

$$\varepsilon = \frac{A\pi\epsilon_0 k}{2k_0^3\Delta} |E^{(p)}E^{(s)*}|, \quad (2.25)$$

$$k = (\mathbf{k}_p - \mathbf{k}_s) \cdot \mathbf{e}_x, \quad (2.26)$$

where \mathbf{e}_x is the unit vector along the x axis, i.e., the axis of weak confinement in the trap.

III. CLASSICAL LIMIT

In the classical limit ($\hat{p} \rightarrow p, \hat{x} \rightarrow x$), the Hamiltonian (2.24) takes the form

$$H = \frac{p^2}{2m} + \frac{m\omega^2 x^2}{2} + \frac{\varepsilon}{k} \cos(kx - \Omega t). \quad (3.1)$$

The classical equations of motion in (p, x) variables are

$$\dot{p} = -\frac{\partial H}{\partial x} = -m\omega^2 x + \varepsilon \sin(kx - \Omega t), \quad \dot{x} = \frac{\partial H}{\partial p} = \frac{p}{m}. \quad (3.2)$$

Equations (3.2) lead to the following second order nonlinear differential equation:

$$\ddot{x} + \omega^2 x = \frac{\varepsilon}{m} \sin(kx - \Omega t). \quad (3.3)$$

A. Dynamics near resonances

Assume that the driving frequency is close to a resonance, i.e.,

$$N\omega \approx \Omega, \quad (3.4)$$

where N is an integer. In this case it is convenient to describe a classical dynamics using the ‘‘action-angle’’ variables [20–22] (I, φ) , which are related to the variables (p, x) by the canonical transformation (see Appendix B)

$$x = \sqrt{\frac{2NI}{\omega m}} \cos\left(\frac{\varphi + \Omega t}{N}\right), \quad p = -\sqrt{2NI\omega m} \sin\left(\frac{\varphi + \Omega t}{N}\right). \quad (3.5)$$

In the variables (I, φ) , the Hamiltonian (3.1) takes the form

$$H = (N\omega - \Omega)I + \frac{\varepsilon}{k} \cos\left(k \sqrt{\frac{2NI}{\omega m}} \cos \Phi - \Omega t\right), \quad (3.6)$$

where

$$\Phi = \frac{\varphi + \Omega t}{N}. \quad (3.7)$$

The second term in Eq. (3.6) can be expanded as a series of Bessel functions $J_n(z)$:

$$\begin{aligned} & \cos\left(k\sqrt{\frac{2NI}{\omega m}}\cos\Phi - \Omega t\right) \\ &= \sum_{n=-\infty}^{\infty} J_n\left(k\sqrt{\frac{2NI}{m\omega}}\right)\cos[n(\Phi + \pi/2) - \Omega t]. \end{aligned} \quad (3.8)$$

We have, for the phase $n(\Phi + \pi/2) - \Omega t$,

$$n(\Phi + \pi/2) - \Omega t = n\frac{\varphi}{N} + \frac{n\pi}{2} + \frac{n-N}{N}\Omega t. \quad (3.9)$$

Thus the classical Hamiltonian (3.6) can be represented in a form where the unperturbed part and the perturbation are explicitly separated,

$$H = H_0 + H_{int}, \quad (3.10)$$

where

$$H_0 = (N\omega - \Omega)I + \frac{\varepsilon}{k}J_N\left(k\sqrt{\frac{2NI}{m\omega}}\right)\cos(\varphi + N\pi/2), \quad (3.11)$$

$$H_{int} = \frac{\varepsilon}{k} \sum_{n \neq N} J_l\left(k\sqrt{\frac{2NI}{m\omega}}\right)\cos\left(\frac{n}{N}\varphi + \frac{n\pi}{2} + \frac{n-N}{N}\Omega t\right). \quad (3.12)$$

In the (I, φ) variables, the classical equations of motion are

$$\begin{aligned} \dot{I} &= -\frac{\partial H}{\partial \varphi} \\ &= \frac{\varepsilon}{k}J_N(z)\sin(\varphi + \pi N/2) \end{aligned} \quad (3.13)$$

$$+ \frac{\varepsilon}{kN} \sum_{n \neq N} nJ_n(z)\sin\left(\frac{n}{N}\varphi + \frac{n\pi}{2} + \frac{n-N}{N}\Omega t\right). \quad (3.14)$$

$$\begin{aligned} \dot{\varphi} &= \frac{\partial H}{\partial I} = N\omega - \Omega + \varepsilon\sqrt{\frac{N}{2m\omega I}}J'_N(z)\cos(\varphi + \pi N/2) \\ &+ \varepsilon\sqrt{\frac{N}{2m\omega I}} \sum_{n \neq N} J'_l(z)\cos\left(\frac{n}{N}\varphi + \frac{n\pi}{2} + \frac{n-N}{N}\Omega t\right), \end{aligned} \quad (3.15)$$

$$+ \varepsilon\sqrt{\frac{N}{2m\omega I}} \sum_{n \neq N} J'_l(z)\cos\left(\frac{n}{N}\varphi + \frac{n\pi}{2} + \frac{n-N}{N}\Omega t\right), \quad (3.16)$$

where

$$z = k\sqrt{\frac{2NI}{m\omega}} \quad (3.17)$$

is a dimensionless variable. Equations (3.14) and (3.16) are convenient when analyzing the classical dynamics in the vicinity of the resonance [Eq. (3.4)]. This case corresponds to small values of ε :

$$\varepsilon < \varepsilon_{cr}. \quad (3.18)$$

Usually, the critical parameter ε_{cr} in Eq. (3.18) should be found numerically (see Sec. V). Under condition (3.18), classical dynamics can be approximately described by the Hamiltonian H_0 [Eq. (3.11)]. The corresponding approximate equations of motion follow from Eqs. (3.14) and (3.16):

$$\dot{I} = -\frac{\partial H}{\partial \varphi} = \frac{\varepsilon}{k}J_N(z)\sin(\varphi + \pi N/2), \quad (3.19)$$

$$\dot{\varphi} = \frac{\partial H}{\partial I} = N\omega - \Omega + \varepsilon\sqrt{\frac{N}{2m\omega I}}J'_N(z)\cos(\varphi + \pi N/2). \quad (3.20)$$

In the general case (for ε large), it is more convenient to use the following exact equations written in (I, φ) variables:

$$\begin{aligned} \dot{I} &= -\frac{\varepsilon}{N}\sqrt{\frac{2NI}{m\omega}}\sin\left[k\sqrt{\frac{2NI}{m\omega}}\cos\left(\frac{\varphi + \Omega t}{N}\right) - \Omega t\right] \\ &\times \sin\left(\frac{\varphi + \Omega t}{N}\right), \end{aligned} \quad (3.21)$$

$$\begin{aligned} \dot{\varphi} &= N\omega - \Omega - \varepsilon\sqrt{\frac{N}{2m\omega I}}\sin\left[k\sqrt{\frac{2NI}{m\omega}}\cos\left(\frac{\varphi + \Omega t}{N}\right) - \Omega t\right] \\ &\times \cos\left(\frac{\varphi + \Omega t}{N}\right). \end{aligned} \quad (3.22)$$

B. Dimensionless variables

To describe both the classical and quantum dynamics, it is convenient to introduce the dimensionless variables

$$\begin{aligned} \tau &= \omega t, \quad \xi = kx, \quad l = \frac{I}{\hbar}, \\ \mathcal{H}_0 &= \frac{H_0}{\hbar\omega}, \quad \mathcal{H}_{int} = \frac{H_{int}}{\hbar\omega}, \quad \mathcal{H} = \frac{H}{\hbar\omega} \end{aligned} \quad (3.23)$$

and the dimensionless parameters

$$\epsilon = \frac{\varepsilon k}{m\omega^2}, \quad \eta^2 = \frac{\hbar k^2}{2m\omega}, \quad \mu = \frac{\Omega}{\omega}, \quad \delta = N - \mu. \quad (3.24)$$

The parameter η is the Lamb-Dicke parameter used in the theory of ion traps to quantify the strength of confinement.

C. Isolated nonlinear resonance

Using Eqs. (3.23) and (3.24), from Eqs. (3.19) and (3.20) we have the approximate dimensionless equations of motion in the vicinity of the resonance (3.4),

$$\frac{dl}{d\tau} = -\frac{\partial \mathcal{H}_0}{\partial \varphi} = \frac{\epsilon}{2\eta^2}J_N(z)\sin(\varphi + \pi N/2), \quad (3.25)$$

$$\frac{d\varphi}{d\tau} = \frac{\partial \mathcal{H}_0}{\partial l} = \delta + \frac{\epsilon}{2\eta}\sqrt{\frac{N}{l}}J'_N(z)\cos(\varphi + \pi N/2), \quad (3.26)$$

where $z = 2\eta\sqrt{Nl}$, and the dimensionless resonant Hamiltonian is

$$\mathcal{H}_0 = l\delta + \frac{\epsilon}{2\eta^2} J_N(z) \cos(\varphi + \pi N/2). \quad (3.27)$$

The classical dynamics corresponding the Hamiltonian (3.27) we shall call “nonlinear resonance.”

To estimate the region of parameters of validity of Eqs. (3.25) and (3.26), their solutions should be compared with the solutions of exact equations (3.21) and (3.22). Equations (3.21) and (3.22) in the dimensionless variables have the forms

$$\frac{dl}{d\tau} = -\frac{\epsilon}{\eta} \sqrt{\frac{l}{N}} \sin\left[z \cos\left(\frac{\varphi + \mu\tau}{N}\right) - \mu\tau\right] \sin\left(\frac{\varphi + \mu\tau}{N}\right), \quad (3.28)$$

$$\frac{d\varphi}{d\tau} = \delta - \frac{\epsilon}{2\eta} \sqrt{\frac{N}{l}} \sin\left[z \cos\left(\frac{\varphi + \mu\tau}{N}\right) - \mu\tau\right] \cos\left(\frac{\varphi + \mu\tau}{N}\right). \quad (3.29)$$

Equations (3.28) and (3.29) are derived from the exact dimensionless Hamiltonian

$$\mathcal{H} = l\delta + \frac{\epsilon}{2\eta^2} \cos\left[z \cos\left(\frac{\varphi + \mu\tau}{N}\right) - \mu\tau\right]. \quad (3.30)$$

In the dimensionless variables (3.23) and (3.24), Eq. (3.3) takes the form

$$\frac{d^2\xi}{d\tau^2} + \xi = \epsilon \sin(\xi - \mu\tau). \quad (3.31)$$

IV. QUANTUM EQUATIONS OF MOTION

In the dimensionless notation [Eqs. (3.23) and (3.24)], the quantum Hamiltonian (2.24) takes the following form in coordinate representation:

$$\frac{\hat{H}}{\hbar\omega} = \mathcal{H} = \frac{1}{2\eta^2} \left[-2\eta^4 \frac{\partial^2}{\partial \xi^2} + \frac{\xi^2}{2} + \epsilon \cos(\xi - \mu\tau) \right]. \quad (4.1)$$

The Schrödinger equation for the Hamiltonian (4.1) is

$$i2\eta^2 \frac{\partial \Psi(\xi, \tau)}{\partial \tau} = [\hat{\mathcal{H}}_{LO} + \epsilon \cos(\xi - \mu\tau)] \Psi(\xi, \tau), \quad (4.2)$$

where $\hat{\mathcal{H}}_{LO}$ is the Hamiltonian of a linear oscillator:

$$\hat{\mathcal{H}}_{LO} = -2\eta^4 \frac{\partial^2}{\partial \xi^2} + \frac{\xi^2}{2}. \quad (4.3)$$

For \hat{h}_0 we have the well-known eigenvalue problem

$$\hat{\mathcal{H}}_{LO}|n\rangle = 2\eta^2(n + 1/2)|n\rangle, \quad (4.4)$$

where

$$|n\rangle \equiv \phi_n(\xi) = \left[\frac{1}{\eta 2^n n! \sqrt{2\pi}} \right]^{1/2} H_n(\xi/\sqrt{2}\eta) e^{-\xi^2/4\eta^2}, \quad (4.5)$$

where $H_n(y)$ is a Hermite polynomial. Although these eigenfunction may appear somewhat unfamiliar because of the use of dimensionless variables, they are in fact the standard eigenfunctions of an unperturbed harmonic oscillator [i.e., the Hamiltonian given by Eq. (2.1) with $\hat{H}_I = 0$]. The normalization condition for the eigenfunction $\phi_n(\xi)$ is

$$\int_{-\infty}^{\infty} \phi_n(\xi) \phi_m(\xi) d\xi = \delta_{n,m}. \quad (4.6)$$

To describe the quantum dynamics we represent the wave function in Eq. (4.2) by the form

$$\Psi(\xi, \tau) = \sum_{n=0}^{\infty} c_n(\tau) \phi_n(\xi). \quad (4.7)$$

From Eq. (4.2) we have the equations for the complex amplitudes, $c_n(\tau)$:

$$\begin{aligned} i \frac{dc_m(\tau)}{d\tau} &= (m + 1/2)c_m(\tau) + \frac{\epsilon}{2\eta^2} \\ &\times \sum_{n=0}^{\infty} \langle m | \cos(\xi - \mu\tau) | n \rangle c_n(\tau) \\ &= (m + 1/2)c_m(\tau) + \frac{\epsilon}{4\eta^2} \sum_{n=0}^{\infty} (e^{-i\mu\tau} F_{m,n}(\eta) \\ &+ e^{i\mu\tau} F_{m,n}^*(\eta)) c_n(\tau). \end{aligned} \quad (4.8)$$

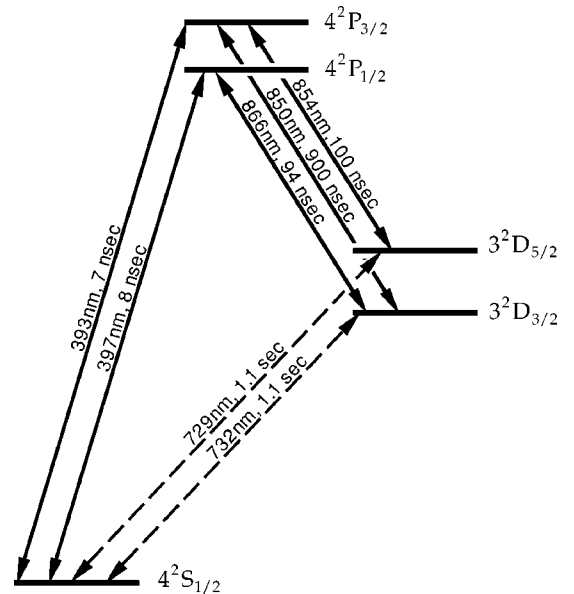


FIG. 3. Energy levels of a Ca⁺ ion. Wavelengths and radiative lifetimes are shown. See Ref. [33] for references.

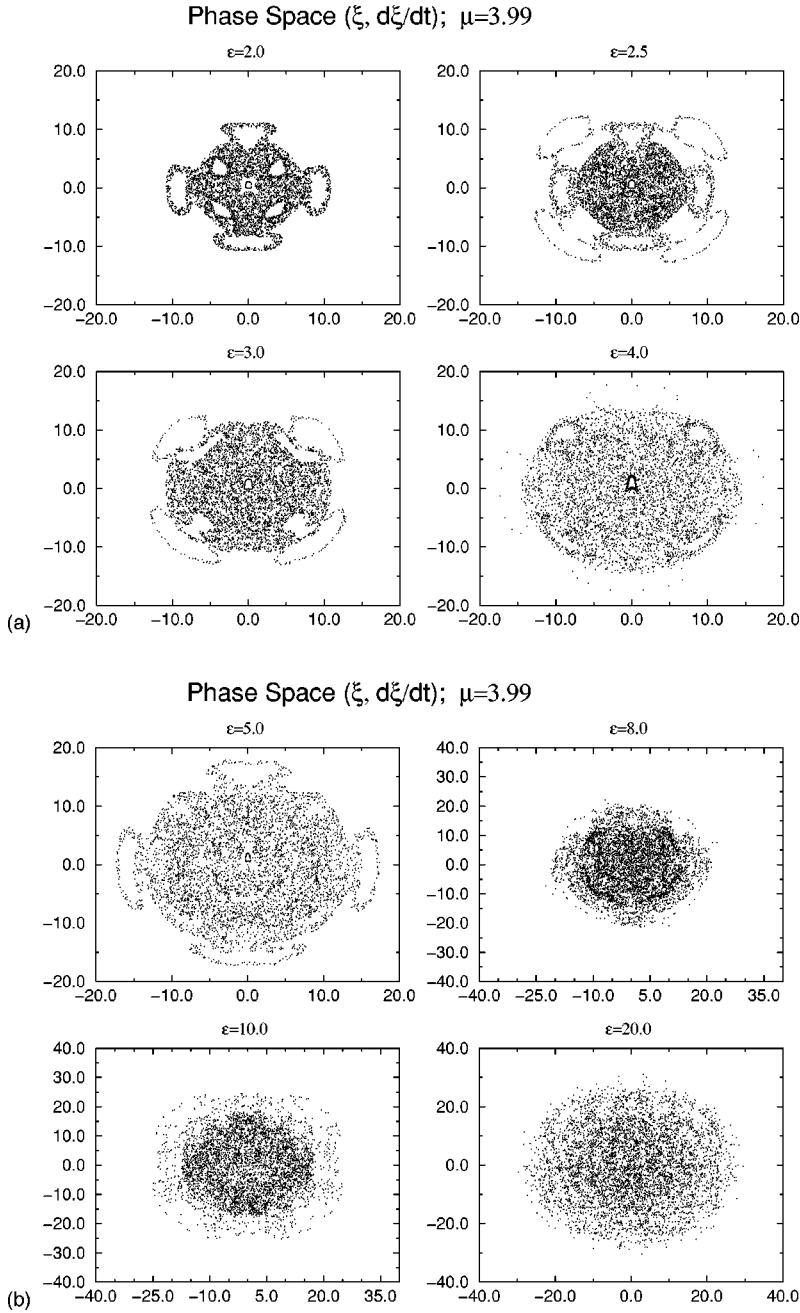


FIG. 4. Classical phase space (Poincaré section). Trajectories with different initial conditions are shown. The values of ϵ are indicated in the figure: (a) $\epsilon=2, 2.5, 3$, and 4 . (b) $\epsilon=5, 8, 10$, and 20 ; $\eta=0.45$; $N=4$ and $\delta=10^{-2}$.

In Eq. (4.8), $F_{m,n}(\eta)$ is the matrix element:

$$F_{m,n}(\eta) = \langle m | e^{i\xi} | n \rangle$$

$$= \frac{1}{\sqrt{\pi 2^{m+n} m! n!}} \int_{-\infty}^{\infty} H_m(u) H_n(u) e^{-u^2 + i 2 \eta u} du. \quad (4.9)$$

Equation (4.8) is used below, in Sec. V, for numerical calculation of the quantum dynamics of the system.

V. RESULTS OF NUMERICAL CALCULATIONS

In this section, we present results of numerical simulations of classical and quantum dynamics of systems whose

Hamiltonians have the form given by Eq. (2.24). We have used a set of parameters which will allow easy experimental verification of our predictions using the type of ion trap apparatus currently being used to investigate quantum computation.

If we use the geometry for the pump and Stokes lasers shown in Fig. 1, the parameter k defined by Eq. (2.26) is given by $k = \cos \theta (k_p + k_s) \approx 2k_0 \cos \theta$. The laser field strengths $|E^{(p)}|$ and $|E^{(s)}|$ can be related to the power in the pump and the Stokes beams, respectively. It is usual to generate one of these beams (the Stokes, say) by frequency modulation of the pump beam, so that the beam parameters will be similar for them both. The power in the pump beam is given by the formula (Ref. [35], p. 488)

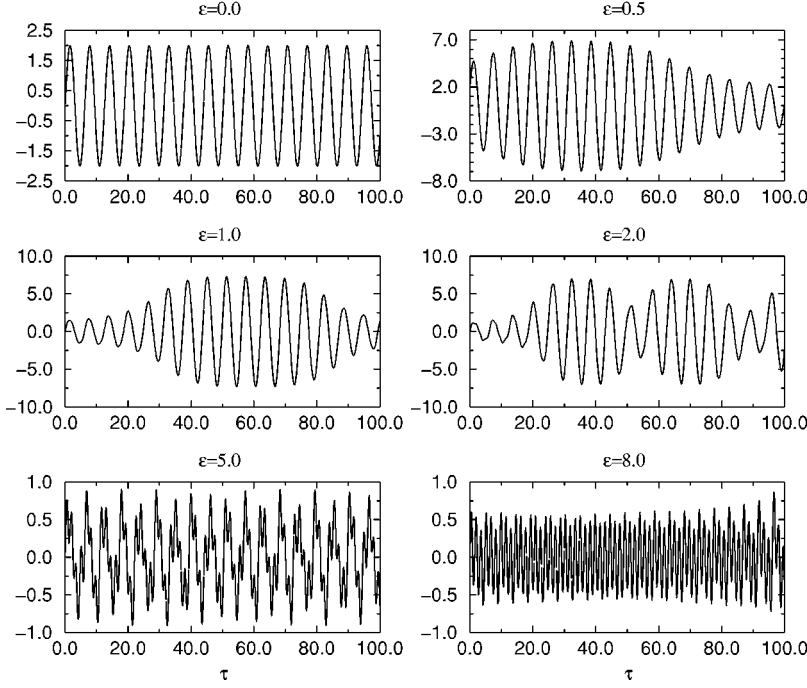
Evolution $\xi(\tau)$; $\mu=3.99$ 

FIG. 5. Time evolution of the dimensionless classical amplitude of oscillations $\xi(\tau)$ for $\epsilon=0, 0.5, 1, 2, 5$, and 8 . The maximum time of simulation is $t_{max}=31.8 \mu s$. Initial condition: $(\xi, d\xi/d\tau)=(0,0)$.

$$P = \frac{c \epsilon_0 \pi}{4} w_0^2 |E^{(p)}|^2, \quad (5.1)$$

where w_0 is the laser spot size (i.e., the $1/e^2$ radius of the intensity distribution). If we substitute this result into Eq. (2.25), we obtain the following expression for the dimensionless parameter ϵ :

$$\epsilon = \frac{\epsilon k}{m \omega^2} = \frac{8AP}{c k_0 m \omega^2 w_0^2 \Delta} s \cos^2 \theta, \quad (5.2)$$

where $s = |E^{(s)}|/|E^{(p)}|$ is a dimensionless parameter of order unity which can be controlled experimentally.

Singly ionized calcium ($m=6.64 \times 10^{-26}$ kg) is common ion in use by several groups worldwide for ion-trap quantum research (see Fig. 3 for energy levels of this ion). For the $^2S_{1/2} \rightarrow ^2P_{1/2}$ transition in this ion (wavelength $\lambda_0=397$ nm) the Einstein A coefficient is [33] $A=1.30 \times 10^8$ s $^{-1}$, and the wave number is $k_0=2\pi/\lambda_0=1.58 \times 10^7$ m $^{-1}$. If we assume a laser power of 10 mW, a spot size $w_0=20$ μ m a trapping frequency $\omega=2\pi \times 500$ kHz, and a detuning $\Delta=2\pi \times 1.0$ GHz, then $\epsilon=1333s \cos^2 \theta$. Thus by varying the experimental free parameters s and θ , one can achieve a large

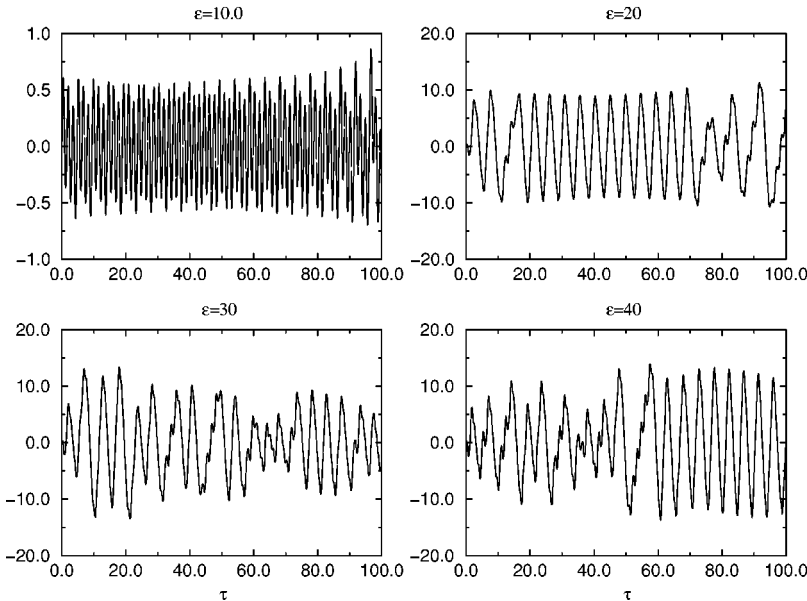
Time Evolution: $\xi(\tau)$; $\mu=3.99$ 

FIG. 6. Chaotic dynamics of the dimensionless classical amplitude of oscillations $\xi(\tau)$ for the values $\epsilon=10, 20, 30$, and 40 . The maximum time of simulation is $t_{max}=31.8 \mu s$. Initial condition: $(\xi, d\xi/d\tau)=(0,0)$.

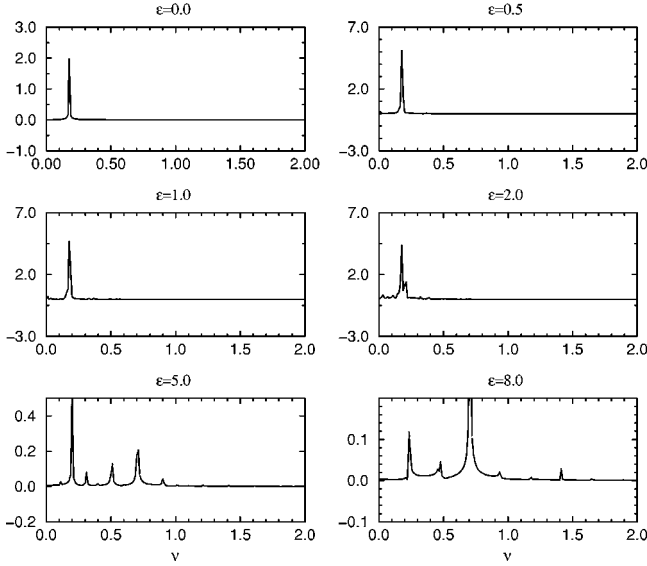
Fourier Transformation: $\text{Re } F[\xi(\tau)](\nu)$; $\mu=3.99$ 

FIG. 7. Frequency Fourier spectrum of the classical amplitude $\xi(\tau)$ for $\epsilon=0, 0.5, 1, 2, 5$, and 8 . The transition to chaos appears at $\epsilon \approx 8$. Initial condition: $(\xi, d\xi/d\tau) = (0, 0)$.

dynamic range for the dimensionless driving force ϵ . The Lamb-Dicke parameter η for these parameters is $0.502 \cos \theta$.

The driving frequency Ω is the difference between the pump and the Stokes frequencies. As mentioned above, these two beams will be realized by splitting one parent beam using a beam splitter and then frequency modulating one of the resultant beam using either an acousto-optic or an electro-optic modulator. In this manner splittings as high as $\Omega = 2\pi \times 100$ MHz can be achieved without too much difficulty, so that the dimensionless parameter N can be in the range 0–200.

A. Simulation of classical dynamics

In Figs. 4(a) and 4(b), the classical phase space (Poincaré section) is shown in the $(\xi, d\xi/d\tau)$ plane, for seven initial conditions, and for different values of the dimensionless driving force ϵ , which characterizes the intensity of the laser beams, and is defined in Eq. (5.2). To derive these results, Eq. (3.31) was solved numerically (for $N=4$ and $\delta=10^{-2}$). These are “stroboscopic” plots, i.e., the values of $(\xi, d\xi/d\tau)$ are plotted for times separated by the dimensionless period: $\omega T = 2\pi\omega/\Omega = 2\pi/\mu$. One can see from Fig. 4(a), that for small values of ϵ ($\epsilon < 2$) the classical dynamics is regular in some regions of the phase space. Note that even at these values of ϵ there exist relatively large regions in the phase space with a chaotic component. When the interaction parameter ϵ increases, the regions with the regular classical dynamics become smaller. As one can see from Fig. 4(a), even at $\epsilon=4$, the dynamics in the region of the phase space corresponding to the “classical ground state” (CGS) [the vicinity of the point (0,0)] remains regular. At larger values of ϵ ($\epsilon \approx 8$) the CGS becomes chaotic. This transition is demonstrated in Fig. 4(b). Figures 5 and 6 show the time evolution of the dimensionless classical coordinate of the ion, $\xi(\tau)$. The maximum dimensionless time of simulations, $\tau_{\max} = 100$, corresponds to the real time scale $t_{\max} = 31.8 \mu\text{s}$ ($\omega = 2\pi \times 500$ kHz). The initial conditions for the dynamics, shown in Figs. 5 and 6 correspond to the CGS. As one can see from Fig. 5, the chaotic component appears at $\epsilon \approx 8$, and is well resolved for $\epsilon > 10$ (see Fig. 6). The frequency Fourier transform for the dynamics, shown in Figs. 5 and 6, is presented in Figs. 7 and 8. It is well known that the transition to the dynamical chaos in classical dynamical systems is accompanied by the transition in the frequency Fourier spectrum. The regular dynamics corresponds to the discrete frequency spectrum, and the chaotic dynamics corresponds to the continuous frequency spectrum. This

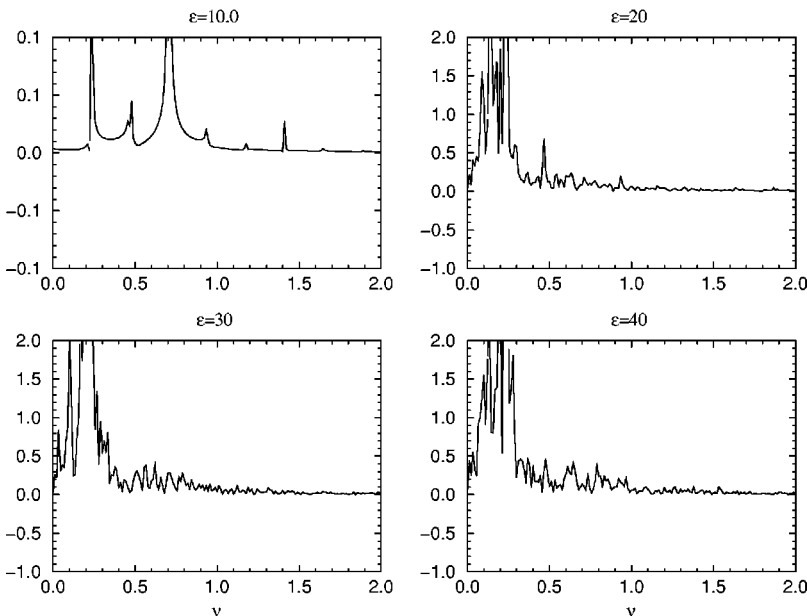
Fourier Transformation: $\text{Re } F[\xi(\tau)](\nu)$; $\mu=3.99$ 

FIG. 8. Frequency Fourier spectrum of the chaotic dynamics of the classical amplitude $\xi(\tau)$ for $\epsilon=10, 20, 30$, and 40 . The transition to chaos appears at $\epsilon \approx 8$. Initial condition: $(\xi, d\xi/d\tau) = (0, 0)$.

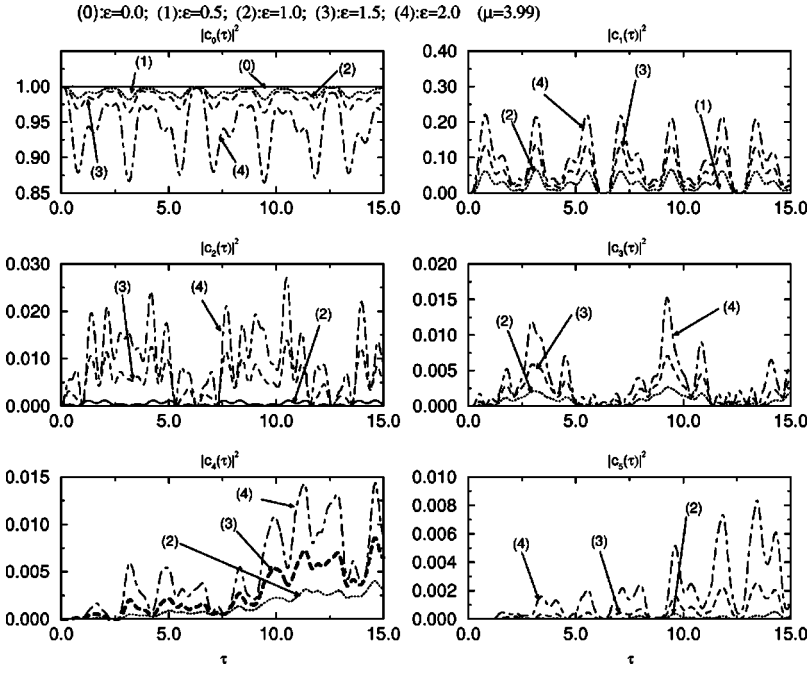


FIG. 9. Dynamics of the quantum probabilities: $P_n(\tau) = |c_n(\tau)|^2$ for $n=0, 1, 2, 3, 4$, and 5 , and $\epsilon=0, 0.5, 1, 1.5$, and 2 . Initial condition: $c_0(0)=1$, $c_n(0)=0$ for $(n>0)$.

characteristic modification of the frequency spectrum is demonstrated in Figs. 7 and 8. For small values of the dimensionless driving force ϵ , one can see only some quasidiscrete lines in the Fourier spectrum. When ϵ increases, the frequency spectrum transforms to a continuous one.

B. Simulation of quantum dynamics

To simulate quantum dynamics, the following parameters were chosen: $N=4$, $\delta=10^{-2}$, and $\eta=0.45$. For the initial conditions we used the ground state of the unperturbed quantum linear oscillator, $c_0(0)=1$ and 0 , for $n>0$. Figure 9

shows the time evolution of the quantum probabilities $P_n(\tau) = |c_n(\tau)|^2$ ($n=0, 1, 2, 3, 4$, and 5) for relatively small values of $\epsilon=0, 0.5, 1, 1.5$, and 2 . These probabilities are quantities which can be measured by tomographic techniques [36]. The values of ϵ correspond to the regular classical dynamics which starts from the CGS. The time evolution of quantum probabilities $P_n(\tau)$ ($n=0, 1, 2$, and 3) for larger values of ϵ is shown in Fig. 10. Because the value of the parameter $\epsilon \approx 8$ corresponds to the classical chaotic dynamics for the initially populated CGS, curves (4) in Fig. 10 describe the quantum chaotic motion. Figure 11 shows the dynamics of the probability function $P_0(\tau)$ for the larger

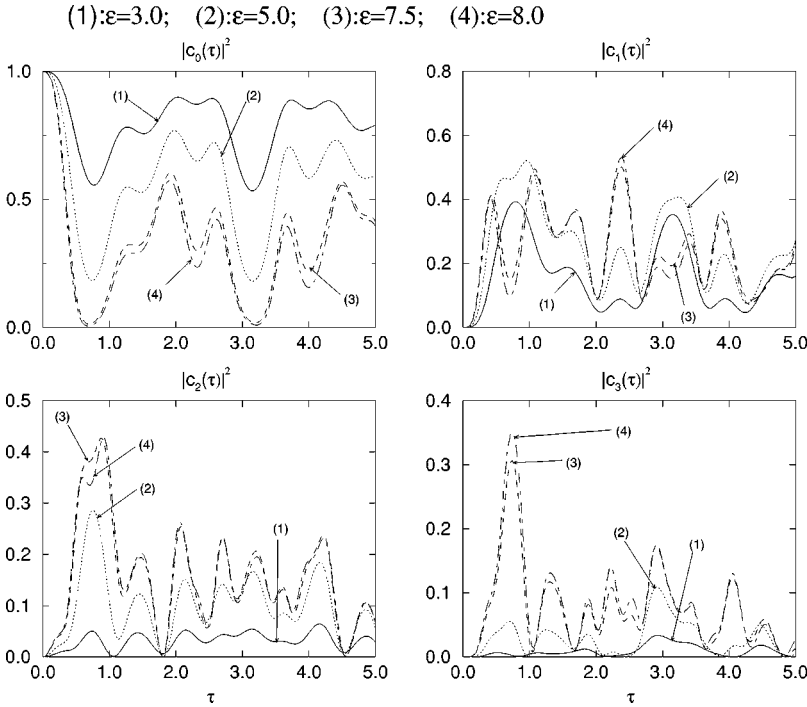


FIG. 10. Dynamics of the quantum probabilities: $P_n(\tau) = |c_n(\tau)|^2$ for $n=0, 1, 2$, and 3 , and $\epsilon=3, 5$, and 7.5 . Initial condition: $c_0(0)=1$, $c_n(0)=0$ for $(n>0)$.

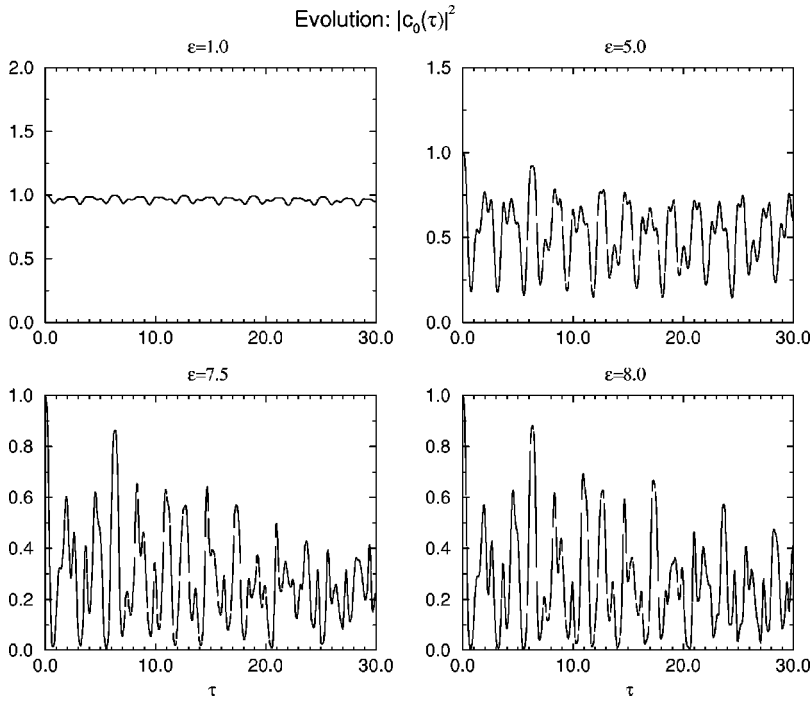


FIG. 11. Dynamics of the quantum probability: $P_0(\tau) = |c_0(\tau)|^2$ for $\epsilon = 1, 5, 7.5$, and 8 . Initial condition: $c_0(0) = 1$, $c_n(0) = 0$ for $(n > 0)$. The transition to quantum chaos corresponds to $\epsilon \approx 8$. The initial conditions are as in Fig. 10.

time interval: $\tau \in [0, 30]$. In real time this corresponds to $t \in [0, 9.54] \mu s$. As one can see from Fig. 11, for $\epsilon > 7.5$ the dynamics of the probability function $P_0(\tau)$ becomes rather complicated, and corresponds to the classical chaotic motion. We hope that this complicated dynamics of the probability functions $P_n(\tau)$ can be measured directly in the experiments with trapped ion. Figure 12 represents the results of the numerical simulations of the frequency Fourier spectrum $P_0(\nu)$ of the quantum probability function $P_0(\tau)$. As one can see from Fig. 12, the characteristic qualitative modification of the frequency spectrum $P_0(\nu)$ starts from $\epsilon > 7.5$. This modi-

fication of the frequency Fourier spectrum can also be measured experimentally. In Fig. 13, we show the results of numerical simulation of the dynamical evolution of the average value, $\langle \xi^2 \rangle \equiv \langle \Psi(\xi, \tau) | \xi^2 | \Psi(\xi, \tau) \rangle$, where the wave function $\Psi(\xi, \tau)$ is defined in Eq. (4.7). This dynamical characteristic is very important for understanding the conditions of stability of the system under consideration, as it describes the amplitude of the ion's oscillations in a trap due to the influence of the resonant laser fields. Experimentally measuring the time dependence of this amplitude is important for characterizing the regular and chaotic dynamics of an ion. The

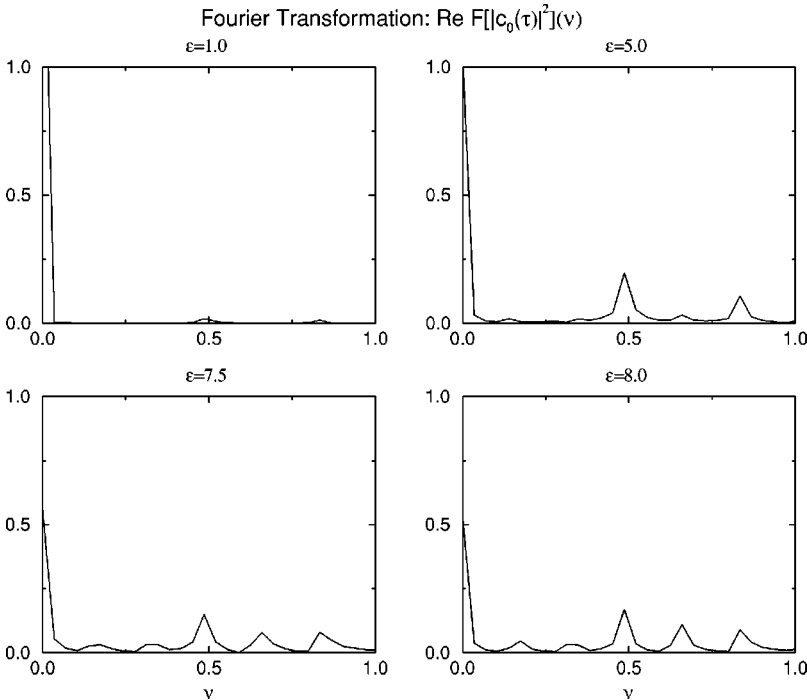


FIG. 12. Frequency Fourier spectrum of the quantum probability: $P_0(\tau) = |c_0(\tau)|^2$ for $\epsilon = 1, 5, 7.5$, and 8 . The transition to chaos appears at $\epsilon \approx 8$. The initial conditions are as in Fig. 10.

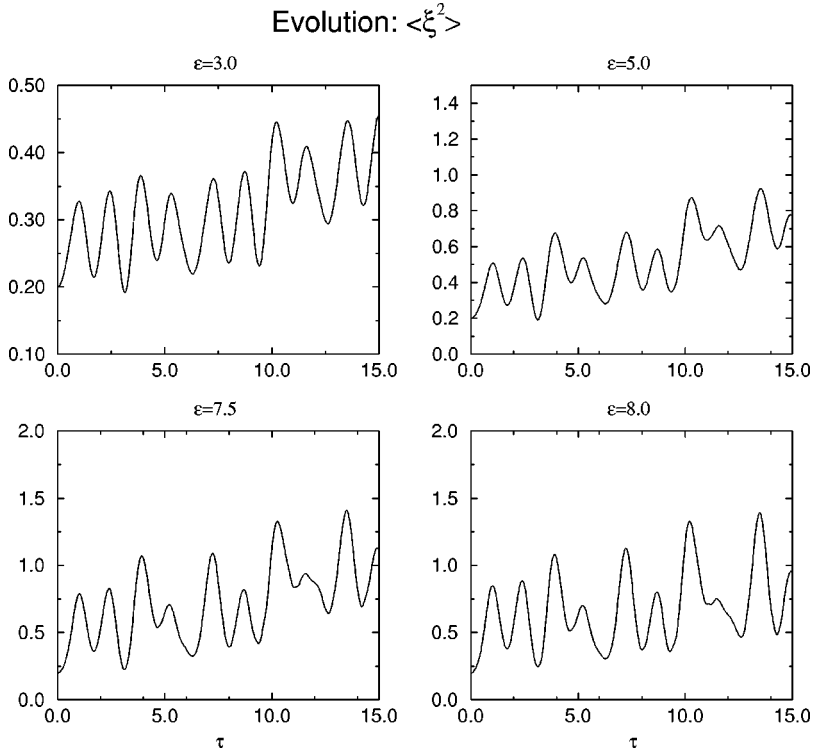


FIG. 13. Dynamical evolution of the average value: $\langle \xi^2 \rangle \equiv \langle \Psi(\xi, \tau) | \xi^2 | \Psi(\xi, \tau) \rangle$, where the wave function $\Psi(\xi, \tau)$ is defined in Eq. (4.7). $\epsilon = 3, 5, 7.5$, and 8 . The transition to chaos appears at $\epsilon \approx 8$. The initial conditions are as in Fig. 10.

frequency spectrum of the amplitude $\langle \xi^2 \rangle$ is shown in Fig. 14 for different values of the perturbation parameter ϵ . As one can see from Fig. 14, at $\epsilon > 7.5$ the frequency spectrum qualitatively modifies, and includes many harmonics. In Fig. 15, we show the time evolution of two functions: the unperturbed Hamiltonian of quantum linear oscillator (4.3), $\langle \hat{\mathcal{H}}_{LO} \rangle$, and the amplitude $\langle \xi^2 \rangle$, for the values of the perturbation parameter: $\epsilon = 0, 0.5$, and 2 . The corresponding classical dynamics is regular in this case. The time evolution of

the same functions is shown in Fig. 16 for larger values of the parameter $\epsilon = 3, 5, 7.5$, and 8 . Curves (3) and (4) correspond to the classically chaotic regime of motion. The maximum simulation time at Fig. 16 is $t_{max} = 4.77 \mu s$.

VI. CONCLUSION

In this paper, we introduced a quantum model which describes a transition from regular dynamics to quantum chaos,

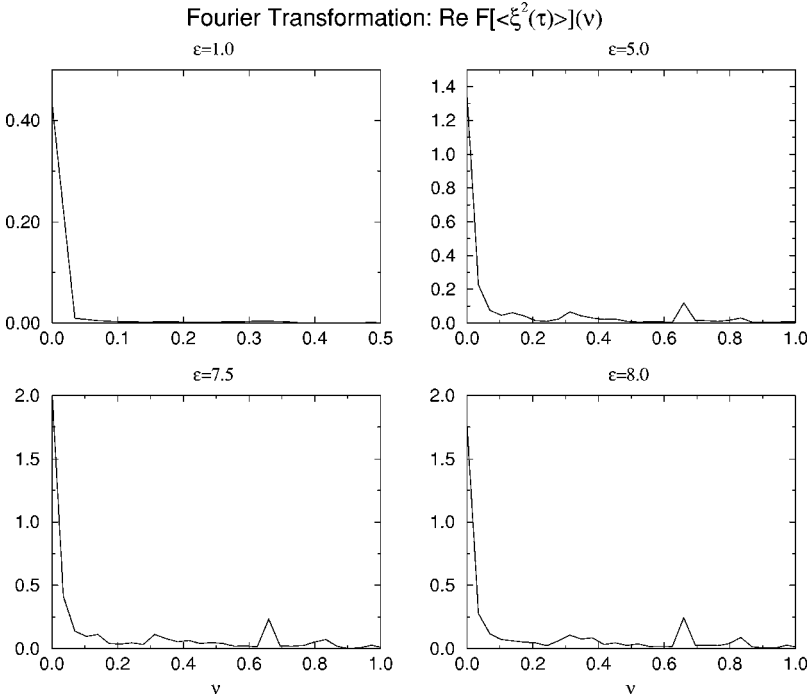


FIG. 14. Frequency Fourier spectrum of the quantum amplitude: $\langle \xi^2 \rangle$, for $\epsilon = 1, 5, 7.5$, and 8 . The transition to chaos appears at $\epsilon \approx 8$. The initial conditions are as in Fig. 10.

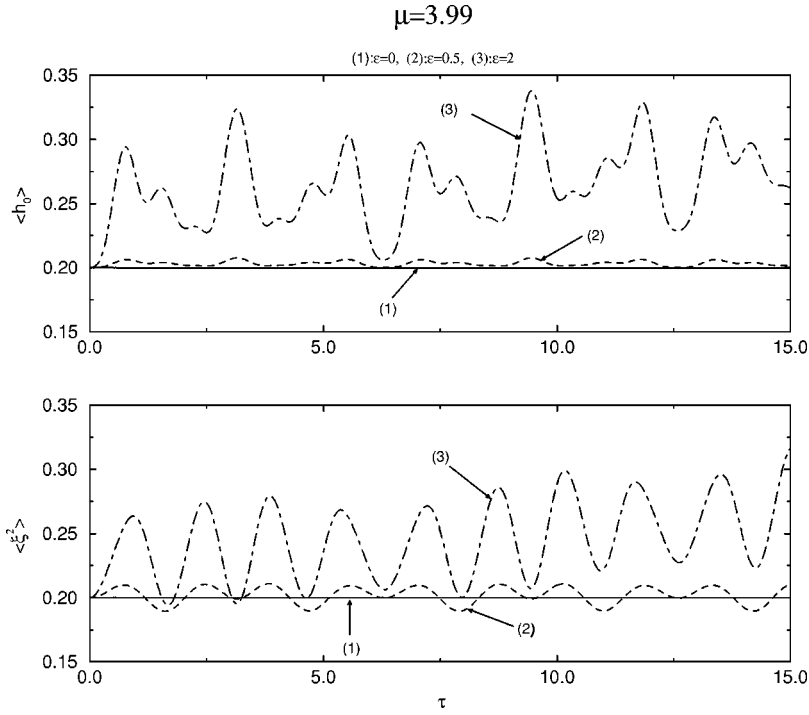


FIG. 15. Time evolution of two functions: the unperturbed Hamiltonian of quantum linear oscillator [Eq. (4.3)], $\langle \hat{h}_{LO} \rangle$, and the amplitude $\langle \xi^2 \rangle$, for the values of the perturbation parameter $\epsilon = 0, 0.5$, and 2 . The corresponding classical dynamics is regular in this case. $\epsilon = 0, 0.5$, and 2 . The initial conditions are as in Fig. 10.

for a single ion in a linear ion trap. The configuration of the resonant laser fields allowed us to represent the model in a “standard” form. That is, our model formally describes a quantum linear oscillator interacting with a one-dimensional plane wave [see Hamiltonian (2.24)]. The classical version of this model is very important and useful in the theory of the dynamical chaos [9]. This model differs significantly from the “usual” nonlinear models (as, for example, a “standard map” [8,10]) considered in theoretical works on dynamical chaos. That is, the model described by the Hamiltonian

(2.24) is degenerate—it includes “nonlinearity” [the term $\cos(kx - \Omega t)$] and a “perturbation parameter” (a parameter ϵ) in the same term in the Hamiltonian (2.24). For these kinds of systems, the *KAM* theory cannot be applied directly, and these systems possess many unusual properties [9]. So quantum analysis of the model described by Hamiltonian (2.24) both theoretically and experimentally will be of significant importance for understanding complicated dynamics in this system, and for applications in different devices based on the trapped ions. The instabilities present in

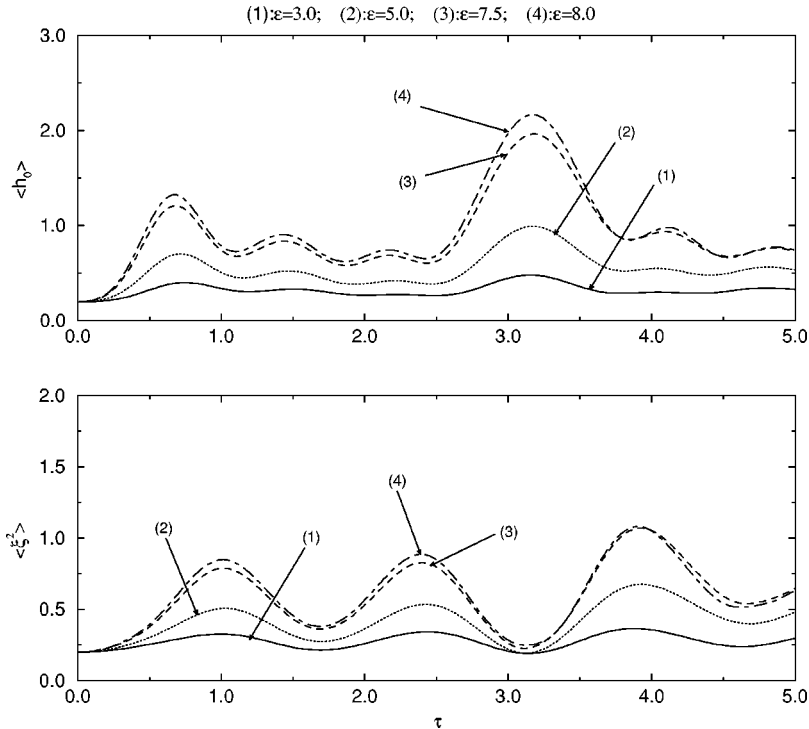


FIG. 16. The time evolution of the same functions shown in Fig. 14, but for larger values of the parameter $\epsilon = 3, 5, 7.5$, and 8 . Curves (3) and (4) correspond to the classically chaotic regime of motion. The initial conditions are as in Fig. 10.

the dynamical model studied here may also play a role in the ion-trap quantum computer, whose dynamics are somewhat different in that the external degrees of freedom are coupled to internal quantum states of the trapped ions (see Ref. [1], and references therein). The numerical results presented in this paper describe both regular and chaotic quantum dynamics, which starts from the initial population of the linear oscillator's ground state. We believe that this regime of motion should be investigated in the experiments with the trapped single ion. These experiments will allow one to establish qualitative and quantitative correspondence between the quantum dynamics described by Hamiltonian (2.29), and the real system of "a single trapped ion plus resonant laser fields." Further theoretical analysis and experiments should include both pure quantum and quasiclassical regions of initial population, and the parameters describing regular and chaotic regimes in both these regions. These investigations are now in progress.

ACKNOWLEDGMENTS

It is a pleasure to thank G.D. Doolen, G. Milburn, and J. Rehacek for valuable discussions. This work was partly supported by the National Security Agency, and by the U.S. Department of Energy under Contract No. W-7405-ENG-36.

APPENDIX A: DERIVATION OF EQ. (2.21)

The dipole matrix elements appearing in Eq. (2.11) can be written in terms of the Einstein A coefficient between the upper and lower manifolds as follows:

$$\langle \mu | \hat{d}_i | \lambda \rangle = \sqrt{\frac{3Ac^2(2J_\lambda + 1)}{4\omega_0^2\alpha}} \sum_{q=-1}^1 \begin{pmatrix} J_\mu & 1 & J_\lambda \\ -m_\mu & q & m_\lambda \end{pmatrix} e_i^{(q)}, \quad (\text{A1})$$

where c is the speed of light, α is the fine-structure constant, ω_0 is the angular frequency of the transition between the upper and lower manifolds, (J_λ, m_λ) are the magnetic quantum numbers for the upper manifold state $|\lambda\rangle$, (J_μ, m_μ) are the magnetic quantum numbers for the lower manifold state $|\mu\rangle$, the term containing six quantities in brackets is the Wigner $3-j$ symbol, and $e_i^{(q)}$ is the i th component of the q th normalized spherical basis vector, viz.

$$\mathbf{e}^{(1)} = -\frac{1}{\sqrt{2}}(1, -i, 0), \quad (\text{A2})$$

$$\mathbf{e}^{(0)} = (0, 0, 1), \quad (\text{A3})$$

$$\mathbf{e}^{(-1)} = \frac{1}{\sqrt{2}}(1, i, 0). \quad (\text{A4})$$

Substituting Eq. (A1) into Eq. (2.11), and assuming that the Zeeman splitting in the upper manifold is small compared to the overall detuning, so that $\Delta_\lambda \approx \Delta$ (independent of λ), then we find that the quantities $\kappa_{\mu,\nu}$ are given by the formula

$$\kappa_{\mu,\nu}(\hat{\mathbf{r}}, t) = \frac{3\pi\epsilon_0 A c^3}{4\omega_0^3 \Delta} \Lambda_{ij}(\mu, \nu) E_i(\hat{\mathbf{r}}, t) E_j^*(\hat{\mathbf{r}}, t), \quad (\text{A5})$$

where the tensor $\Lambda_{ij}(\mu, \nu)$ is given by

$$\Lambda_{ij}(\mu, \nu) = (2J_\lambda + 1) \sum_{m_\lambda=-J_\lambda}^{J_\lambda} \sum_{q,q'=-1}^1 \begin{pmatrix} J_\mu & 1 & J_\lambda \\ -m_\mu & q & m_\lambda \end{pmatrix} \times \begin{pmatrix} J_\nu & 1 & J_\lambda \\ -m_\nu & q' & m_\lambda \end{pmatrix} e_i^{(q)} e_j^{(q')*}. \quad (\text{A6})$$

If we assume that the lower manifold is the $^2S_{1/2}$ ground state of an alkali ion, the two states being denoted $|1\rangle = ^2S_{1/2}, m = -1/2$ and $|2\rangle = ^2S_{1/2}, m = 1/2$, and that the upper manifold is the $^2P_{1/2}$ state, then these tensors can be found in closed forms:

$$\Lambda_{ij}(1,1) = \Lambda_{ij}^*(2,2) = \frac{1}{3} \begin{pmatrix} 1 & -i & 0 \\ i & 1 & 0 \\ 0 & 0 & 1 \end{pmatrix}, \quad (\text{A7})$$

$$\Lambda_{ij}(1,2) = -\Lambda_{ij}^*(2,1) = \frac{1}{3} \begin{pmatrix} 0 & 0 & -1 \\ 0 & 0 & -i \\ 1 & i & 0 \end{pmatrix}.$$

Therefore the cross products involving the electric field components with these tensors can be written as follows:

$$\Lambda_{ij}(1,1) E_i E_j^* = \frac{1}{3} [|\mathbf{E}|^2 + 2 \text{Im}\{E_X E_Y^*\}], \quad (\text{A8})$$

$$\Lambda_{ij}(2,2) E_i E_j^* = \frac{1}{3} [|\mathbf{E}|^2 - 2 \text{Im}\{E_X E_Y^*\}], \quad (\text{A9})$$

$$\Lambda_{ij}(1,2) E_i E_j^* = \frac{1}{3} [E_Z(E_X^* + iE_Y^*) - E_Z^*(E_X + iE_Y)], \quad (\text{A10})$$

$$\Lambda_{ij}(2,1) E_i E_j^* = \frac{1}{3} [-E_Z(E_X^* - iE_Y^*) + E_Z^*(E_X - iE_Y)]. \quad (\text{A11})$$

If these results are substituted into the definition of h_0 and h_i , Eqs. (2.17)–(2.20), one obtains Eq. (2.21). Similar results, with slightly different numerical factors, are obtained if the upper manifold is a $^2P_{3/2}$ state.

APPENDIX B: CANONICAL TRANSFORM TO "ACTION-ANGLE" VARIABLES

The theory of canonical transforms in classical mechanics is described in detail in Ref. [37], Sec. 45. We want to transform from a set of variable x, p to a new set φ, I , where φ plays the role of position coordinate and I the role of momentum. Such transforms are specified by a *generating function* $F(x, \varphi, t)$. Then variables p and I and the Hamiltonian in

the new coordinate system are related to F by the formulas

$$p = \frac{\partial F}{\partial x}, \quad (\text{B1})$$

$$I = -\frac{\partial F}{\partial \varphi}, \quad (\text{B2})$$

$$H(\varphi, I) = H(x, p) + \frac{\partial F}{\partial t}. \quad (\text{B3})$$

For the canonical transform used in Sec. III A, the generating function is given by

$$F(x, \varphi, t) = -\frac{m\omega}{2}x^2 \tan\left(\frac{\varphi + \Omega t}{N}\right). \quad (\text{B4})$$

Substituting, we find

$$p = -m\omega x \tan\left(\frac{\varphi + \Omega t}{N}\right), \quad (\text{B5})$$

$$I = -\frac{m\omega}{2N}x^2 \sec^2\left(\frac{\varphi + \Omega t}{N}\right), \quad (\text{B6})$$

$$H(\varphi, I) = H(x, p) - \frac{m\omega\Omega}{2N}x^2 \sec^2\left(\frac{\varphi + \Omega t}{N}\right) \quad (\text{B7})$$

$$= H(x, p) - \Omega I. \quad (\text{B8})$$

Equation (B5) implies that

$$x = \sqrt{\frac{2NI}{m\omega}} \cos\left(\frac{\varphi + \Omega t}{N}\right). \quad (\text{B9})$$

On substitution of this last formula into Eq. (B6), we obtain

$$p = -\sqrt{2Nm\omega I} \sin\left(\frac{\varphi + \Omega t}{N}\right). \quad (\text{B10})$$

-
- [1] R. J. Hughes, D. F. V. James, J. J. Gomez, M. S. Gulley, M. H. Holzschelter, P. G. Kwiat, S. K. Lamoreaux, C. G. Peterson, V. D. Sandberg, M. M. Schauer, C. M. Simmons, C. E. Thorburn, D. Tupa, P. Z. Wang, and A. G. White, *Fortschr. Phys.* **46**, 329 (1998).
 - [2] G. P. Berman, G. D. Doolen, R. Mainieri, and V. I. Tsifrinovich, *Introduction to Quantum Computers* (World Scientific, Singapore, 1998).
 - [3] G. P. Berman and G. M. Zaslavsky, *Physica A* **91**, 450 (1978).
 - [4] G. P. Berman and G. M. Zaslavsky, in *Quantum Chaos*, edited by G. Casati and B. Chirikov (Cambridge University Press, Cambridge, 1995), p. 435.
 - [5] G. P. Berman, E. N. Bulgakov, and D. D. Holm, *Crossover-Time in Quantum Boson and Spin Systems* (Springer-Verlag, Berlin, 1994).
 - [6] G. P. Berman and G. M. Zaslavsky, *Phys. Lett. A* **61**, 295 (1977).
 - [7] B. V. Chirikov (unpublished).
 - [8] B. V. Chirikov, *Phys. Rep.* **52**, 263 (1979).
 - [9] G. M. Zaslavsky, *Chaos in Dynamic Systems* (Harwood, New York, 1985).
 - [10] A. Lichtenberg and M. Leiberman, *Regular and Chaotic Motion* (Springer, New York, 1983).
 - [11] G. P. Berman, G. M. Zaslavsky, and A. R. Kolovsky, *Zh. Éksp. Teor. Fiz.* **81**, 506 (1981) [*Sov. Phys. JETP* **54**, 272 (1981)].
 - [12] G. P. Berman and A. R. Kolovsky, *Usp. Fiz. Nauk* **162**, 205 (1992) [*Sov. Phys. Usp.* **35**, 303 (1992)].
 - [13] G. P. Berman, O. F. Vlasova, and F. M. Izrailev, *Zh. Éksp. Teor. Fiz.* **93**, 470 (1987) [*Sov. Phys. JETP* **66**, 269 (1987)].
 - [14] G. P. Berman and A. R. Kolovsky, *Zh. Éksp. Teor. Fiz.* **95**, 1553 (1989) [*Sov. Phys. JETP* **68**, 818 (1989)].
 - [15] G. P. Berman, E. N. Bulgakov, and D. D. Holm, *Phys. Rev. A* **52**, 3074 (1995).
 - [16] G. P. Berman, E. N. Bulgakov, D. K. Campbell, and I. V. Krive, *Phys. Rev. B* **56**, 10 338 (1997).
 - [17] G. P. Berman and A. R. Kolovsky, *Phys. Lett. A* **125**, 188 (1987).
 - [18] L. E. Reichl, *The Transition to Chaos in Conservative Classical Systems: Quantum Manifestations* (Springer-Verlag, Berlin, 1992).
 - [19] J. E. Bayfield, S. Y. Luie, L. C. Perotti, and M. P. Skrzypkowski, *Phys. Rev. A* **53**, R12 (1996).
 - [20] G. M. Zaslavsky, R. Z. Sagdeev, D. A. Usikov, and A. A. Chernikov, *Weak Chaos and Quasi-Regular Patterns* (Cambridge University Press, Cambridge, 1992).
 - [21] A. A. Chernikov, R. Z. Sagdeev, D. A. Usikov, M. Yu. Zakharov, and G. M. Zaslavsky, *Nature (London)* **326**, 559 (1987).
 - [22] A. A. Chernikov, M. Ya. Natenzon, B. A. Petrovichev, R. Z. Sagdeev, and G. M. Zaslavsky, *Phys. Lett. A* **129**, 377 (1998).
 - [23] J. K. Breslin, C. A. Holmes, and G. J. Milburn, *Phys. Rev. A* **56**, 3022 (1997).
 - [24] G. P. Berman, V. Yu. Rubaev, and G. M. Zaslavsky, *Nonlinearity* **4**, 543 (1991).
 - [25] M. Frasca, *Phys. Lett. A* **231**, 344 (1997).
 - [26] S. A. Gardiner, J. I. Cirac, and P. Zoller, *Phys. Rev. Lett.* **79**, 4790 (1997).
 - [27] B. G. Klappauf, W. H. Oskay, D. A. Steck, and M. G. Raizen, *Phys. Rev. Lett.* **81**, 1203 (1998).
 - [28] B. G. Klappauf, W. H. Oskay, D. A. Steck, and M. G. Raizen, *Phys. Rev. Lett.* **81**, 4044 (1998).
 - [29] C. Monroe, D. M. Meekhof, B. E. King, and D. J. Wineland, *Science* **272**, 1131 (1996).
 - [30] D. J. Wineland, C. Monroe, D. M. Meekhof, B. E. King, D. Leibfried, W. M. Itano, J. C. Bergquist, D. Berkeland, J. J. Bollinger, and J. Miller, *Proc. R. Soc. London, Ser. A* **454**, 411 (1998).

- [31] M. Roberts, P. Taylor, G. P. Barwood, P. Gill, H. A. Klein, and W. R. C. Rowley, *Phys. Rev. Lett.* **78**, 1876 (1997); D. J. Berkeland, J. D. Miller, J. C. Bergquist, W. M. Itano, and D. J. Wineland, *ibid.* **80**, 2089 (1998).
- [32] J. I. Cirac and P. Zoller, *Phys. Rev. Lett.* **74**, 4091 (1995); C. Monroe, D. M. Meekhof, B. E. King, W. M. Itano, and D. J. Wineland, *ibid.* **75**, 4714 (1995).
- [33] D. F. V. James, *Appl. Phys. B: Photophys. Laser Chem.* **66**, 181 (1998).
- [34] B. W. Shore, *The Theory of Coherent Atomic Excitation* (Wiley, New York, 1990).
- [35] P. W. Milonni and J. H. Eberly, *Lasers* (Wiley, New York, 1988).
- [36] D. Leibfried, D. M. Meekhof, C. Monroe, B. E. King, W. M. Itano, and D. J. Wineland, *J. Mod. Opt.* **44**, 2485 (1997).
- [37] L. D. Landau and E. M. Lifshitz, *Mechanics* (Pergamon, Oxford, 1960).